Resonance anlaysis of e^+e^- annihilation

D. Horn*
Institute for Advanced Study, Princeton, New Jersey 08540

Daniel E. Novoseller
California Institute of Technology, Pasadena, California 91125
and TRW/DSSG, Redondo Beach, California 90278 †

(Received 27 April 1978)

We present a formalism of overlapping resonances with variable channel structure which is suitable for the analysis of inclusive and exclusive data in e^+e^- annihilation into hadrons. We use it in a discussion of the $\psi'(3.68)$ and $\psi''(3.77)$ states, in a fit to SPEAR data in the range 3.9–4.1 GeV and a fit to DESY data in the range 4.0–4.3 GeV. Two fits to the SPEAR data are used as examples of various features of the resonance system. Special attention is paid to the contraint that a very strong channel ($D^*\bar{D}^*$) opens up in the middle of the resonance structure. Both inclusive and exclusive quantities are displayed and the correlation between them is discussed.

I. INTRODUCTION

Precision experiments in the resonance regions of e^+e^- annihilation can yield very interesting information about the structure of the relevant hadronic systems. We present and discuss a method for the analysis of such data. This problem is analogous to phase-shift analysis in that an effort is made to reconstruct scattering amplitudes from cross sections. It is, however, different from phase-shift analysis in many respects. Whereas the latter method is applied to a situation in which one hadronic scattering channel is investigated and several partial waves are allowed, here we are faced with one partial wave ($J^{PC}=1^{--}$), but we would like to include information from many hadronic channels. The method that we discuss is based on the idea that a limited number of overlapping resonances is produced by the virtual photon and they decay into all open hadronic channels. The analysis allows in principle for the most general structure in the production and decay of the resonance system, the only input being the number of resonances used as a basis for the analysis.

We review in Sec. II the general formalism that is used to describe the production of two overlapping resonances by the virtual photon and their decay into hadronic channels. This formalism was described in Ref. 1 and is based on the Weisskopf-Wigner[2] analysis of overlapping resonances carried out in Ref. 3. The analysis of Refs. 1 and 3 used the assumption that there is no important structure in the decay channels within the range of the resonance system. We relax this assumption in our analysis in Sec. II. We allow for energy variations such as the opening of a strong decay channel in the energy range which is being analyzed. The result is that the effective Hamiltonian, whose eigenvalues describe the locations of the resonances, becomes energy dependent. Using an explicit Schrödinger equation we demonstrate that the effective mass and width obey a dispersion relation.

As a first application we discuss in Sec. III the system of $\psi'(3.68)$ and $\psi''(3.77)$. All hadronic decay channels of $\psi'(3.68)$ are strongly suppressed and for the purpose of our analysis it may be regarded as a zero-width resonance with an appreciable coupling to the photon. The $\psi''(3.77)$ has a much weaker coupling to the photon, but its hadronic width is large since it lies above the $D\bar{D}$ threshold at 3.73 GeV. Neglecting this width one can use the available data to determine the structure of the mass matrix. We discuss the conditions under which this analysis is valid in light of the formalism developed in Sec. II.

Section IV contains a resonance analysis of the available SLAC data in the range 3.9–4.1 GeV. This serves as a demonstration of the technique. We regard it, however, premature to use our best fit—in spite of its impressive χ^2—as a final determination of the physical parameters. We show, therefore, two fits which have different characteristics to demonstrate the general features of possible solutions that can be obtained in a two-resonance analysis of this region.

Our final application is to recent DESY data in the (4.0–4.3)-GeV region. We show in Sec. V that these data can be nicely fitted by incoherent Breit-Wigner shapes. This fit does not necessitate the whole apparatus developed in Sec. II. We expect the general form of the resonance analysis to be most useful when interference effects are necessary to explain a complicated energy behavior of the cross section.

A short discussion of our technique and the physical implications of our results is given in Sec. VI.

II. GENERAL FORMALISM

The inclusive description of a system of two overlapping resonances can be most succinctly parametrized by an effective Hamiltonian,[3]

$$\underline{H}=\underline{M}-\tfrac{1}{2}i\underline{\Gamma}\ , \tag{1}$$

which is a 2×2 matrix in the Hilbert space spanned by the two resonance states. The two matrices $\underline{M}$ and $\underline{\Gamma}$ are Hermitian. If the interactions are invariant under time reversal, the two matrices become symmetric in the proper T-invariant vector basis. Since, in general, the two matrices $\underline{M}$ and $\underline{\Gamma}$ do not commute, $\underline{H}$ cannot be diagonalized by a unitary transformation. As a result, the two right eigenvectors $|\mathrm{I}\rangle$ and $|\mathrm{II}\rangle$, which obey

$$\underline{H}|\mathrm{I}\rangle=\epsilon_1|\mathrm{I}\rangle,\quad \underline{H}|\mathrm{II}\rangle=\epsilon_2|\mathrm{II}\rangle,$$
$$\epsilon_{1,2}=M_{1,2}-\tfrac{1}{2}i\Gamma_{1,2}\ , \tag{2}$$

will not be orthogonal to one another. Therefore, the two left eigenvectors

$$\langle\mathrm{I}'|\underline{H}=\langle\mathrm{I}'|\epsilon_1,\quad \langle\mathrm{II}'|\underline{H}=\langle\mathrm{II}'|\epsilon_2 \tag{3}$$

will not be the Hermitian conjugates of the right eigenvectors. In the T-invariant case we can relate these two sets of states by time reversal,

$$T|\mathrm{I}\rangle=|\mathrm{I}'\rangle,\quad T|\mathrm{II}\rangle=|\mathrm{II}'\rangle\ . \tag{4}$$

Moreover, one can solve for one set of states in terms of the other and obtain

$$|\mathrm{I}'\rangle=\frac{|\mathrm{I}\rangle-\chi|\mathrm{II}\rangle}{(1-|\chi|^2)^{1/2}}\ ,$$
$$|\mathrm{II}'\rangle=\frac{|\mathrm{II}\rangle-\chi^*|\mathrm{I}\rangle}{(1-|\chi|^2)^{1/2}}\ , \tag{5}$$

where χ is the overlap

$$\chi=\langle\mathrm{II}|\mathrm{I}\rangle\ . \tag{6}$$

The choice of phases determined by (4) and (5) leads to a purely imaginary overlap χ. These results were discussed at length in Ref. 3. Using Eq. (5) one obtains the representation of $\underline{H}$ in terms of these vectors:

$$\underline{M}-\tfrac{1}{2}i\underline{\Gamma}=\frac{\epsilon_1|\mathrm{I}\rangle\langle\mathrm{I}'|}{(1-|\chi|^2)^{1/2}}+\frac{\epsilon_2|\mathrm{II}\rangle\langle\mathrm{II}'|}{(1-|\chi|^2)^{1/2}}\ . \tag{7}$$

Since we deal with strong interactions we will assume time-reversal invariance and express the eigenvectors in terms of T-invariant orthonormal basis vectors $|1\rangle$ and $|2\rangle$:[1]

$$|\mathrm{I}\rangle=\frac{1}{(\cosh2y)^{1/2}}\,(\cos z|1\rangle+\sin z|2\rangle)\ ,$$
$$|\mathrm{II}\rangle=\frac{1}{(\cosh2y)^{1/2}}\,(-\sin z|1\rangle+\cos z|2\rangle)\ , \tag{8}$$

where z is a complex parameter:

$$z=x+iy\ . \tag{9}$$

The other set of vectors will be obtained by using the antiunitary T operation as specified by Eq. (4):

$$|\mathrm{I}'\rangle=\frac{1}{(\cosh2y)^{1/2}}\,(\cos z^*|1\rangle+\sin z^*|2\rangle)\ ,$$
$$|\mathrm{II}'\rangle=\frac{1}{(\cosh2y)^{1/2}}\,(-\sin z^*|1\rangle+\cos z^*|2\rangle)\ . \tag{10}$$

It is then easy to check that the orthogonality conditions

$$\langle\mathrm{I}'|\mathrm{II}\rangle=0,\quad \langle\mathrm{II}'|\mathrm{I}\rangle=0 \tag{11}$$

hold, and the overlap (6) is the purely imaginary number,

$$\chi=i\tanh2y\ . \tag{12}$$

The six parameters of the complex matrix $\underline{H}$ can thus be replaced by the two complex eigenvalues ϵ_1 and ϵ_2 and the two real parameters x and y. All these parameters may, in general, be energy dependent. The problem is much simplified in the narrow-resonance approximation in which one assumes that all these parameters are constant (or do not vary considerably over the small energy range where the effect of the resonances is observed). In this case the energy dependence of any cross section which involves these two resonances has a structure of two Breit-Wigner distributions interfering with one another. The overlap χ can then be given a simple intuitive meaning.[3] It can be written as

$$\chi=\chi_{\mathrm{BW}}\chi_c\ , \tag{13}$$

where χ_{BW} is the overlap of two Breit-Wigner distributions

$$\chi_{\mathrm{BW}}=\frac{i(\Gamma_1\Gamma_2)^{1/2}}{\epsilon_2^*-\epsilon_1} \tag{14}$$

and χ_c designates an overlap in the space of decay channels, i.e., $|\chi_c|$ represents the degree to which the decay channels of the two states match one another. This leads then to the constraint

$$|\chi|\le|\chi_{\mathrm{BW}}|\ , \tag{15}$$

which may also be derived from the physical requirement that $\underline{\Gamma}$ be a positive-definite matrix, since the latter leads to the relation

$$\det\underline{\Gamma}=\frac{\Gamma_1\Gamma_2}{1-|\chi|^2}\left(1-\frac{|\chi|^2}{|\chi_{\mathrm{BW}}|^2}\right)\ . \tag{16}$$

All this formalism follows simply from treating the quantum-mechanical problem of production and decay of resonances in the Weisskopf-Wigner (WW) approximation.[2] Let us sketch it briefly for the case of a single resonance. The generalization to a system of many resonances is straightforward. In the interaction representation, one considers the effect of an interaction Hamiltonian H' on the time development of a wave function described by the eigenfunctions of some H_0 that consist of a discrete level with probability amplitude $a_R(t)$ and a continuum with probability amplitudes $a_i(E_c, t)$. One assumes that H' has nonvanishing matrix elements only between the resonance and the continuum. This is the WW approximation. Under this assumption one obtains a closed solution of the resonance problem. In principle there is no loss of generality in diagonalizing first the continuum sector and regarding the remainder as H', but in simple models one includes in H_0 only free states. The WW approximation means then that the interactions between continuum channels proceed always through resonance states.

The Schrödinger equation turns into the following set of equations:

$$\begin{aligned} i\dot{a}_j(E_c) &= H'_{jR}(E_c)a_R e^{i(E_c - M_0)t} \ , \\ i\dot{a}_R &= \sum_j \int \rho_j(E_c)H'_{Rj}(E_c)a_j(E_c) \\ &\quad \times e^{i(M_0 - E_c)t}dE_c \ , \end{aligned} \tag{17}$$

where M_0 is the eigenvalue of H_0 corresponding to the discrete level R. If we choose the boundary conditions at $t = -\infty$ as

$$a_R \xrightarrow[t\to-\infty]{} 0, \quad a_i(E_c) \xrightarrow[t\to-\infty]{} \frac{\alpha_i}{\rho_i(E_c)}\delta(E_c - E) \ , \tag{18}$$

then we may follow the time development of the system and deduce from the coefficients at $t = +\infty$,

$$\sqrt{\rho_i}\, a_i(t = +\infty) = S_{ij}\sqrt{\rho_j}\, a_j(t = -\infty) \ , \tag{19}$$

the value of the S matrix at the energy E, $S_{ij}(E)$. Note that E was introduced by the boundary conditions (18). The solution to Eqs. (17) and (18) is given explicitly by

$$\begin{aligned} a_R(t) &= \sum_i H'_{Ri}(E)\alpha_i \frac{e^{i(M_0 - E)t}}{E - M(E) + \frac{1}{2}i\Gamma(E)} \ , \\ a_i(E_c, t) &= \frac{\alpha_i}{\rho_i(E_c)}\delta(E_c - E) \\ &\quad - \frac{iH'_{iR}(E_c)\sum_j \alpha_j H'_{Rj}(E)}{E - M(E) + \frac{1}{2}i\Gamma(E)} \frac{e^{i(E_c - E)t}}{i(E_c - E) + \epsilon} \ , \end{aligned} \tag{20}$$

where $M(E)$ and $\Gamma(E)$ are given by

$$\begin{aligned} \Gamma(E) &= \sum_i 2\pi\rho_i(E)|H'_{Ri}(E)|^2 , \\ M(E) &= M_0 + \frac{1}{2\pi}\,\mathrm{P}\int \frac{\Gamma(E')dE'}{E - E'} \ . \end{aligned} \tag{21}$$

Finally, the S matrix is given by

$$S_{ij} = \delta_{ij} - \frac{i\Gamma(E)P_{ij}(E)}{E - M(E) + \frac{1}{2}i\Gamma(E)} \ , \tag{22}$$

where P_{ij} is the projection operator

$$P_{ij}(E) = \frac{2\pi}{\Gamma(E)}\,[\rho_i(E)\rho_j(E)]^{1/2}H'_{iR}(E)H'_{Rj}(E) \ . \tag{23}$$

The connection between this quantum-mechanical problem and the S-matrix formalism of overlapping resonances was discussed at length in Ref. 3. Many related discussions exist in the literature.[4] We have indulged in this exercise here in order to derive the energy-dependent dispersion relation Eq. (21) and to establish the connection between the inclusive formalism of the effective Hamiltonian and the couplings to exclusive decay channels.

Equation (22) is unitary, as required of an S matrix. Although this S matrix has in principle only one pole at some complex value of E, one may regard $M(E) - \frac{1}{2}i\Gamma(E)$ as the effective pole at the energy E. Similar statements hold for the two-resonance systems which we discussed at the beginning of this section. In the narrow-resonance approximation $\rho(E)$ and $H'_{iR}(E)$ are assumed to be constant in the region $|E - M| < \Gamma$. We cannot use this approximation in all our applications since we will encounter situations in which a very strong decay channel opens up in the middle of a resonance structure. Let us therefore discuss the mathematical structure that emerges from our formalism in the case in which only one decay channel has significant energy dependence. If this channel is a two-body decay channel with angular momentum l and threshold energy E_{th}, we should expect

$$\begin{aligned} &\rho \sim k\theta(E - E_{\mathrm{th}}), \quad H' \sim k^l \ , \\ &k(E) \equiv \tfrac{1}{2}(E^2 - E_{\mathrm{th}}^2)^{1/2} \ , \end{aligned} \tag{24}$$

and, in a single-resonance problem,

$$\Gamma = \Gamma_0 + 2\pi k^{2l+1}g(k)\theta(E - E_{\mathrm{th}}); \quad g(0) \neq 0 \ . \tag{25}$$

Correspondingly the mass will be

$$M = M_0 + \mathrm{P}\int_{E_{\mathrm{th}}}^{\infty} \frac{k^{2l+1}(E')g(k(E'))dE'}{E - E'} \ . \tag{26}$$

Alternatively it can be represented in the subtracted form

$$M(E)=M(E_{\rm th})+(E_{\rm th}-E)\,\mathrm{P}\int_{E_{\rm th}}^{\infty}\frac{k^{2l+1}(E')g(k(E'))dE'}{(E-E')(E_{\rm th}-E')}\,. \quad (27)$$

In the case of a two-resonance problem both $\underline{M}$ and $\underline{\Gamma}$ will be matrices, related by the dispersion relation (21). Since only one channel is assumed to contribute to the variation of $\underline{\Gamma}$ and $\underline{M}$, they will not have three independent coupling functions $g(k)$ but only two. The reason is that any single decay channel contribution to the width matrix factorizes:

$$(\langle 1|\Gamma^i|2\rangle)^2=\langle 1|\Gamma^i|1\rangle\langle 2|\Gamma^i|2\rangle\,. \quad (28)$$

Γ^i designates the contribution of the ith channel to the width matrix which is written here explicitly in the basis introduced above in Eq. (8).

A clear distinction should be made between the two different Hilbert spaces which we use to describe a resonance system. One space is that of their production and decay channels, within which the S matrix is defined. The other is the basis of the effective Hamiltonian. The dimension of the S matrix is determined by the number of different decay channels whereas the dimension of the basis of the Hamiltonian is the number of resonances in question. Although the S matrix is the one which is directly related to experimental observations, it is often very useful to discuss the resonance system in the effective Hamiltonian Hilbert space. This is the basis in which the resonances are most easily described within models such as the quark model, whose underlying structure is different from the observed decay products. Moreover, whenever only inclusive information is available, one cannot determine coupling parameters beyond those of $\underline{H}$. The inclusive production of hadrons in e^+e^- annihilation lends itself most easily to a description in terms of the Hamiltonian language. A single resonance contributes to the ratio R of the hadronic cross section divided by the $\mu^+\mu^-$ cross section the amount

$$\Delta R=\frac{3\pi}{f^2}E\frac{\Gamma}{(E-M)^2+\frac{1}{4}\Gamma^2}\,. \quad (29)$$

In this expression it was assumed that the coupling of the photon to the vector meson is $(e/f)M^2$ and the hadronic width Γ is much larger than Γ_{ee} and, therefore, represents also the total width. In the case of two overlapping resonances the virtual photon couples to the two states that span the Hilbert space of $\underline{H}$. Whatever the couplings are, one linear combination of these states decouples from the photon. Without any loss of generality, we will assume henceforth that the state $|2\rangle$ decouples from the photon and, therefore, only $|1\rangle$ is produced in e^+e^- annihilation. This leads to the following expression for ΔR:[1]

$$\Delta R=\frac{3\pi}{f^2}E\frac{1}{1-|\chi|^2}\left[\frac{\Gamma_1|\langle I'|1\rangle|^2}{|E-\epsilon_1|^2}+2\,\mathrm{Re}\frac{i\chi(\epsilon_1-\epsilon_2^*)\langle 1|II'\rangle\langle I'|1\rangle}{(E-\epsilon_2^*)(E-\epsilon_1)}+\frac{\Gamma_2|\langle II'|1\rangle|^2}{|E-\epsilon_2|^2}\right]. \quad (30)$$

When the narrow-resonance approximation is valid the various parameters are constants and the integral of the cross section determines the e^+e^- width of the state $|1\rangle$:

$$\int\frac{M^2}{E^2}\Delta R\,dE=\frac{6\pi^2}{f^2}M=\frac{9\pi}{2\alpha^2}\Gamma_{e^+e^-}\,. \quad (31)$$

In general, however, the various parameters may be energy dependent and should be fitted locally at each energy. Finally, using Eq. (10) we can rewrite Eq. (30) using the parameters x and y:

$$\Delta R=\frac{3\pi}{f^2}E\frac{1}{1-|\chi|^2}\left\{\frac{1}{|E-\epsilon_1|^2}\left[\tfrac{1}{2}\Gamma_1\left(1+\frac{\cos 2x}{\cosh 2y}-\tanh^2 2y\right)+(E-M_1)\frac{\sin 2x}{\cosh 2y}\tanh 2y\right]\right.$$
$$\left.+\frac{1}{|E-\epsilon_2|^2}\left[\tfrac{1}{2}\Gamma_2\left(1-\frac{\cos 2x}{\cosh 2y}-\tanh^2 2y\right)-(E-M_2)\frac{\sin 2x}{\cosh 2y}\tanh 2y\right]\right\}. \quad (32)$$

This is the expression that we will use to fit the experimental data. The six parameters deduced from these fits, i.e., $M_{1,2}=\mathrm{Re}\epsilon_{1,2}$, $\Gamma_{1,2}=-2\,\mathrm{Im}\epsilon_{1,2}$, x and y, can be used to reconstruct the six parameters which define the matrix elements of the complex symmetric effective Hamiltonian, Eq. (1). The explicit connections between these two equivalent sets of parameters are given in the Appendix.

III. ANALYSIS OF THE $\psi'(3.68)$ - $\psi''(3.77)$ SYSTEM

The ψ'' state[5] lies above the threshold of the $D\bar{D}$ continuum (3.73 GeV) and below the next continuum channel of $D\bar{D}^*$ (3.87 GeV). It has a hadronic width of $\Gamma=28\pm 7$ MeV and an e^+e^- width of $\Gamma_{e^+e^-}=0.37\pm 0.10$ keV. The latter is considerably smaller than $\Gamma_{e^+e^-}=2.1\pm 0.3$ keV of the $\psi'(3.68)$. It seems consistent to think of these two levels as

mixtures of an S-D charmonium structure. In the notation introduced above we will then use the charmonium identification

$$|1\rangle = |2^3S_1\rangle, \quad |2\rangle = |1^3D_1\rangle, \qquad |\mathrm{I}\rangle = |\psi'(3.68)\rangle, \quad |\mathrm{II}\rangle = |\psi''(3.77)\rangle . \tag{33}$$

$\psi''(3.77)$ is then produced in e^+e^- annihilation via the component $|1\rangle$ in its state vector. Using Eq. (8) we find that the size of this probability amplitude, which we will denote by $\sin\alpha$, is

$$\sin\alpha \equiv \frac{|\sin z|}{(\cosh 2y)^{1/2}} = \left[\tfrac{1}{2}\left(1 - \frac{\cos 2x}{\cosh 2y}\right)\right]^{1/2} . \tag{34}$$

From the experimental values of Γ_{ee} for the two states, it follows that[5]

$$\alpha = 23^\circ \pm 3^\circ . \tag{35}$$

As explained in the preceding section, the eigenstates $|\mathrm{I}\rangle$ and $|\mathrm{II}\rangle$ will stay constant over the energy range of interest only provided there is no violent change in the decay structure within that same region. In this example an important decay channel opens up in between the masses of the two states. Let us nonetheless first ignore the $\underline{\Gamma}$ matrix, find out the structure of the $\underline{M}$ matrix, and then ask ourselves how stable these results are once the decay effects are properly taken into account.

If $\underline{\Gamma}$ is neglected we may use all the information stated above to determine $\underline{M}$:

$$\underline{M} = \begin{pmatrix} 3.70 & \pm 0.03 \\ \pm 0.03 & 3.76 \end{pmatrix} \mathrm{GeV} . \tag{36}$$

Fishbane *et al.*[6] have argued that the choice of a positive sign in M_{12} leads to the conclusion that the effective tensor force that can cause such an off-diagonal term has the same strength as the one deduced from the splittings of the observed 1^3P_J levels. We will compare this result of

$$M_{12} \simeq 30 \text{ MeV} \tag{37}$$

with the M_{12} matrix elements that we will deduce from our fits to the resonance structures observed at higher masses.

The angle α is measured at the location of $\psi''(3.77)$ where $\underline{\Gamma} \neq 0$. It is then quite plausible that $M_1 = \mathrm{Re}\epsilon_1$ evaluated at $E = 3.77$ GeV will be different from 3.68. This can come about either from energy variation of $\underline{M}$ over this region or from the explicit introduction of $\underline{\Gamma}$. To find the relative importance of these two effects let us first estimate the parameter y. Since we deal here with a one-channel system, $\det\underline{\Gamma} = 0$ and

$$\tanh^2 2y = |\chi|^2 = |\chi_{\mathrm{BW}}|^2 = \frac{\Gamma_1\Gamma_2}{(M_1 - M_2)^2 + \frac{1}{4}(\Gamma_1 + \Gamma_2)^2} . \tag{38}$$

This result follows from Eqs. (12), (13), and (14). (See also the Appendix.) Γ_2 is the measured width of ψ'', $\Gamma_2 \approx 0.03$ GeV, but Γ_1 is completely unknown. Γ_1 is the width attributed to the state $|\mathrm{I}\rangle$ above threshold. Since, however, M_1 is below threshold it will hardly be a visible effect, producing only a small variation in the background of the ψ'' Breit-Wigner shape.

Let us assume, for simplicity, that $\Gamma_1 \leq \Gamma_2$. In that case, and if $|M_1 - M_2|$ does not change considerably from the observed value of 0.09 GeV, it follows from Eq. (38) that $\tanh^2 2y \leq 0.1$. Hence, y is quite small. Using the equalities [the first follows from Eq. (34) and the second is given in the Appendix]

$$\cos 2x = \cos 2\alpha \cosh 2y , \tag{39}$$

$$2M_{12} = (M_1 - M_2)\sin 2x \cosh 2y + \tfrac{1}{2}(\Gamma_1 - \Gamma_2)\cos 2x \sinh 2y , \tag{40}$$

we find that for small values of y

$$x \approx \pm\alpha , \tag{41}$$

$$2M_{12} \approx \pm(M_1 - M_2)\sin 2\alpha . \tag{42}$$

Moreover, the quantity $M_1 - M_2$ obeys the equality (see the Appendix)

$$(M_1 - M_2)(\cosh^2 2y - \sin^2 2x) = (M_{11} - M_{22})\cos 2x \cosh 2y + \tfrac{1}{2}(\Gamma_{11} - \Gamma_{22})\sin 2x \sinh 2y , \tag{43}$$

which for small values of y reduces to

$$(M_1 - M_2) \approx \frac{M_{11} - M_{22}}{\cos 2\alpha} . \tag{44}$$

The conclusion is that as long as Γ_1 and Γ_2 are $\leq \frac{1}{3}|M_1 - M_2|$, only the variations of $\underline{M}$ are relevant to the evaluation of α. Moreover, it should be expected that if $\underline{\Gamma}$ is small, its effects on $\underline{M}$ via the dispersion relation (21) are small too, and $M_1 - M_2$ as well as M_{12} will not vary considerably.

The situation is different if $\Gamma_1 > \Gamma_2$. As noted above, we do not have direct physical information about Γ_1 at $E = 3.77$ GeV. If, for some mysterious reason, it turns out to be much larger than Γ_2, the derivation of M_{12} is inoperative. As an example, we plot in Fig. 1 the variation of M_{12} vs Γ_1/Γ_2 for the case $M_1 - M_2 = M_{\psi''} - M_{\psi'}$. α was kept fixed at $\alpha = 23^\circ$ and the sign of M_{12} was chosen to be positive. For a qualitative understanding of what is happening, let us discuss the case in which

only the state $|1\rangle$ is allowed to couple to the hadronic decay channel $(D\bar{D})$, i.e., $\Gamma_{12}=\Gamma_{22}=0$. Using $\alpha=23°$ we find $\Gamma_1=5.6\Gamma_2$. Using $|M_1-M_2|=0.09$ GeV it follows that $\tanh^2 2y\approx 0.3$. As a result the second term on the right-hand side of Eq. (40) will be more than half as large as the first term and the two possible results for M_{12} (corresponding to the two different signs of x) show large deviations from 0.03 GeV. Within a conventional charmonium picture the coupling of the photon depends on the wave function at the origin, and, therefore, only state $|1\rangle$ couples to it. But the decay into $D\bar{D}$ is a nonlocal process, i.e., the new $q\bar{q}$ pair can be produced for arbitrary configurations of the c and $\bar{c}$. Therefore, this hypothetical example with $\Gamma_{12}=\Gamma_{22}=0$ is, in fact, unreasonable. It, furthermore, seems reasonable to assume that Γ_1 will indeed be of the same size as Γ_2 and, while the result $M_{12}=30$ MeV is not exact, it is still a reasonable estimate of the magnitude of this matrix element in the ψ'-ψ'' system.

It should be noted that a recent publication from SLAC,[7] by a different group from Ref. 5, claims that $\Gamma_{e^+e^-}(\psi'')=180\pm 60$ eV. This is $\frac{3}{5}$ of the result of Ref. 5 that we used in our analysis, and should therefore lead to a corresponding reduction of $\tan^2\alpha$. M_{12} is then reduced to 24 MeV.

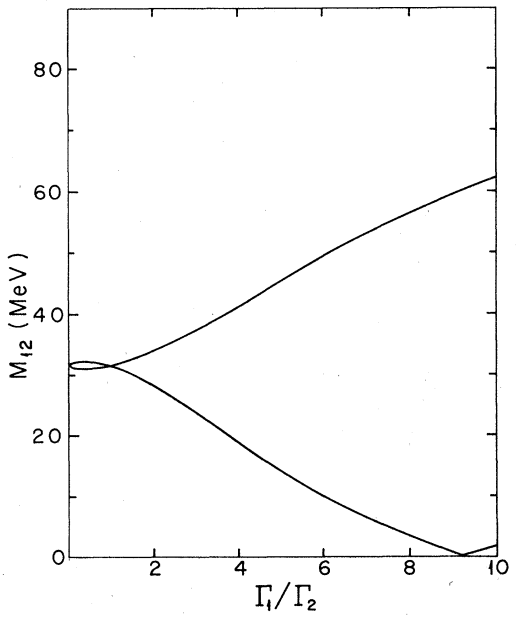

FIG. 1. Variation of M_{12} as a function of Γ_1/Γ_2 in the ψ'-ψ'' system. The fixed parameters are $\alpha=23°$ and $M_2-M_1=0.09$ GeV. There exist also solutions in which the sign of M_{12} is negative and its absolute value is the same as shown here.

IV. ANALYSIS OF THE (3.9-4.1)-GeV REGION

The SPEAR data that were obtained in the Mark I detector[8] show a very sharp increase in R immediately above 4 GeV. This feature, together with the two peaks at ~3.96 and 4.03 GeV, can be described by an overlapping resonance structure. An inclusive analysis of these data in terms of Eq. (30) with constant values of $\underline{H}$ was performed by Dothan and Horn.[1] It allows for two different classes of solutions: (A) Two resonances with comparable widths (of about 65 MeV) whose masses are close to the observed peaks of R. (B) A narrow resonance ($\Gamma\simeq 20$ MeV) located at about the same mass (~4 GeV) as a broad resonance ($\Gamma\simeq 200$ MeV) and interfering destructively with it. Since this inclusive analysis had been performed an important new experimental fact was discovered. The $D^*\bar{D}^*$ channel, which opens up at about 4.012 GeV, couples very strongly[9] to the resonating system at 4.028 GeV. To be more specific, the detected events that can be identified with $D^{0*}\bar{D}^{0*}$ production and eventual decays have a cross section which is of the same order of magnitude as those events that can be attributed to $D^0\bar{D}^{0*}+\bar{D}^0D^{0*}$. The third available channel, $D\bar{D}$, seems to play a relatively small role at this energy. This experimental observation leads to the interesting question whether and how the opening of this strong new channel modifies the analysis of the data and its consequences. In this section we address this question.

To establish the mathematical structure of the needed formalism, let us investigate first the case of two interfering resonances in the presence of two decay channels. We use the notation

$$(2\pi\rho_A)^{1/2}\langle 1|H'|A\rangle=a_1e^{i\alpha},\quad (2\pi\rho_B)^{1/2}\langle 1|H'|B\rangle=b_1e^{i\beta}, \tag{45}$$

$$(2\pi\rho_A)^{1/2}\langle 2|H'|A\rangle=a_2e^{i\alpha},\quad (2\pi\rho_B)^{1/2}\langle 2|H'|B\rangle=b_2e^{i\beta},$$

where A and B are the two decay channels in question. The matrix elements of $\underline{\Gamma}$ in the T-invariant basis will then be

$$\Gamma_{ij}=a_ia_j+b_ib_j\ . \tag{46}$$

Since the parameters a_i and b_i are chosen to be real, the diagonal matrix elements of $\underline{\Gamma}$ are positive but Γ_{12} may have either sign depending on the relative signs of a_1 and a_2 and of b_1 and b_2. Note also that

$$\det\underline{\Gamma}=(a_1b_2-b_1a_2)^2\geq 0 \tag{47}$$

and vanishes if there is only a single decay eigenchannel. The contribution of a particular channel (e.g., A) to the production amplitude is proportional to

$$\frac{(2\pi\rho_A)^{1/2}}{(1-|\chi|^2)^{1/2}}\left\langle A\left|H'\left(\frac{|\mathrm{I}\rangle\langle\mathrm{I}'|}{E-\epsilon_1}+\frac{|\mathrm{II}\rangle\langle\mathrm{II}'|}{E-\epsilon_2}\right)\right|1\right\rangle \quad (48)$$

when only the component $|1\rangle$ couples to the photon. Using the notation[3] for the decay amplitude of the resonance $|\mathrm{I}\rangle$ into channel A,

$$(\gamma_1^A)^{1/2}=(a_1\langle 1|\mathrm{I}\rangle+a_2\langle 2|\mathrm{I}\rangle)e^{-i\alpha}=\frac{e^{-i\alpha}}{(\cosh 2y)^{1/2}}(a_1\cos z+a_2\sin z) \quad (49)$$

(where $\gamma_{\mathrm{I}}^A\equiv\langle A|T|\mathrm{I}\rangle$), we find that the cross section of channel A will be

$$\sigma_A=\frac{4\pi^2\alpha^2}{f^2E}\cosh 2y\left[\left|\frac{\gamma_{\mathrm{I}}^A\cos z}{E-\epsilon_1}\right|^2+\left|\frac{\gamma_{\mathrm{II}}^A\sin z}{E-\epsilon_2}\right|^2-\mathrm{Re}\,\frac{(\gamma_{\mathrm{I}}^{A*}\gamma_{\mathrm{II}}^A)^{1/2}(i\sinh 2y+\sin 2x)}{(E-\epsilon_{\mathrm{I}}^*)(E-\epsilon_2)}\right]. \quad (50)$$

A similar equation holds for σ_B. The generalization to a three-channel problem is straightforward: One defines parameters c_i in analogy to a_i and b_i. Γ_{ij} will have an additional contribution of c_ic_j and $|\gamma_{\mathrm{I}}^C|$ as well as σ_C can be determined in terms of c_i and the other parameters of the problem. The sum of all cross sections divided by $\sigma(e^+e^-\to\mu^+\mu^-)=4\pi\alpha^2/3E^2$ gives the inclusive result of Eq. (30).

A threshold behavior in ρ_A at E_{th} will cause γ^A and σ_A to vanish for $E<E_{\mathrm{th}}$. This variation will change the other cross sections too, since $\underline{\Gamma}$ will be energy dependent, thus affecting $\underline{M}$ via Eq. (21) and making all parameters energy dependent. In our analysis we have parametrized the energy dependence in the form

$$a_ia_j=2\pi\alpha_i\alpha_j\,\frac{(E^2-E_0^2)^{3/2}\exp-[(E-E_0)/E_1]}{E(E^2-E_0^2+4\mu^2)}\times\theta(E-E_0), \quad (51)$$

where $\alpha_{i,j}$ are constants and the following values were assigned to the parameters:

$$E_0=4.0114\ \mathrm{GeV},\quad E_1=1\ \mathrm{GeV},\quad \mu=0.2\ \mathrm{GeV}. \quad (52)$$

E_0 is chosen as $2M_{D^{*0}}$.[10] μ is the Blatt-Weisskopf barrier mass as conventionally used in πN phase-shift analyses.[11] This threshold behavior is appropriate for a p-wave decay (into $D^*\bar{D}^*$) starting at $E_{\mathrm{th}}=E_0$. The exponential damping factor was used to enforce convergence of the dispersion relations for the mass matrix. Our formulas for $\underline{H}$ become

$$\Gamma_{ij}=a_ia_j+b_ib_j+c_ic_j,\qquad M_{ij}=M_{ij}^0+\frac{1}{2\pi}\mathrm{P}\int\frac{a_ia_j(E')dE'}{E-E'}, \quad (53)$$

where b_i, c_i, and M_{ij}^0 are constants.

From experimental data at $E=4.028$ GeV one can conclude that

$$\sigma_A:\sigma_B:\sigma_C=0.48\pm0.12:0.46\pm0.1:0.06\pm0.03,$$

where A, B, and C denote the channels $A=D^{*0}\bar{D}^{*0}$, $B=D^0\bar{D}^{*0}+\bar{D}^0D^{*0}$, $C=D^0\bar{D}^0$. Using isospin invariance one would expect the same ratios to hold for the total $I=0$ combinations of charmed mesons obtained from the decays of the charmonium system. There is, however, the problem that the mass of the D^{*+} is about 4 MeV higher than that of D^{*0}, hence $D^{*+}D^{*-}$ production should be suppressed compared to $D^{*0}\bar{D}^{*0}$. Since it is difficult to estimate the exact value of the $D^{*+}D^{*-}$ contribution, and we do not want to increase the error on this constraint in order not to lose its qualitative effect on our fit, we use

$$\sigma_A:\sigma_B=1\pm0.35,\quad \sigma_C:\sigma_B=0.13\pm0.07\ \text{at}\ 4.028\ \mathrm{GeV}, \quad (54)$$

where $A=D^*\bar{D}^*$, $B=D\bar{D}^*+D^*\bar{D}$, $C=D\bar{D}$. In this way we may have overemphasized the role of the D^*D^* channel. This is, however, consistent with the purpose of our discussion in this section, namely, finding out how the strong opening of a strong channel affects the resonance analysis.

On the experimental data for R we have to perform several subtractions to account for effects which are not due to the resonances that we study. We relate ΔR of Eq. (32) to R that we fit by

$$\Delta R=R-B-\Delta R_\tau-\Delta R_{\mathrm{HM}}. \quad (55)$$

B is assumed to be a constant background due to noncharm production. Its value is left free and gets determined by the fit. ΔR_τ represents the amount contributed by $\tau^+\tau^-$ production as estimated in Ref. 12:

$$\Delta R_\tau\approx 0.89\left(1-\frac{4m_\tau^2}{E^2}\right)^{1/2}\left(1+\frac{2m_\tau^2}{E^2}\right),\qquad m_\tau=1.9\ \mathrm{GeV}. \quad (56)$$

We have not included the errors of the parameters in Eq. (56) since they are of marginal importance to our analysis. ΔR_{HM} is the possible contribution to the energy region in question from the tails of resonances located at higher energies. In the fits presented here we use

$$\Delta R_{\mathrm{HM}}=\frac{3\pi}{f^2}E\,\frac{\Gamma}{(E-M)^2+\frac{1}{4}\Gamma^2}, \quad (57)$$

where f and $\Gamma_{e^+e^-}$ are related by Eq. (31), and

$$M=4.164\ \mathrm{GeV},\quad \Gamma=46\ \mathrm{MeV},\quad \Gamma_{e^+e^-}=0.45\ \mathrm{keV}. \quad (58)$$

are the parameters of the high-mass resonance of the DASP data in our incoherent fit in the next section [see Eqs. (66) and (67)].

The three terms on the right-hand side of Eq. (54) amount to a subtraction of a smoothly varying background from the fitted R curve. This subtracted curve rises slowly toward the upper part of the fitted energy region ($3.9 < E < 4.1$ GeV). The major part of this rise is due to ΔR_{HM}. The qualitative details of our fits are not affected by this smoothly varying background which we will display together with our fits to R.

Our fitting program is based on an optimization technique which involves minimizing the χ^2 function,

$$\chi^2 = \sum_{i=1}^{N} \left[\frac{R_{\mathrm{data}}(E_i) - R_{\mathrm{theory}}(E_i)}{\Delta R_{\mathrm{data}}} \right]^2 + \left(\frac{f_{\mathrm{data}} - f_{\mathrm{theory}}}{\Delta f_{\mathrm{data}}} \right)^2 + \left(\frac{g_{\mathrm{data}} - g_{\mathrm{theory}}}{\Delta g_{\mathrm{data}}} \right)^2 , \tag{59}$$

where N is the number of data points and

$$\left.\begin{aligned} f &= R(e^+e^- \to D^*\bar{D}^*)/R(e^+e^- \to D\bar{D}^* + D^*\bar{D}) \\ g &= R(e^+e^- \to D\bar{D})/R(e^+e^- \to D\bar{D}^* + D^*\bar{D}) \end{aligned}\right\} \text{ at } E = 4.028 \text{ GeV}. \tag{60}$$

The theoretical functions of our fit were discussed above. They are presented in terms of energy-independent parameters A_i which are changed by the program to obtain the best fit. The search for the best fit is based on the error matrix

$$M_{ij} = \frac{\partial^2 \chi^2}{\partial A_i \partial A_j} . \tag{61}$$

The error of the parameter A^i is defined by

$$\Delta A^i = [(M^{-1})_{ii}]^{1/2} . \tag{62}$$

The parameters may be strongly correlated by nondiagonal matrix elements of M_{ij}. For a given set of parameters $\{A_i^0\}$ the program finds a better estimate $\{A_i^1\}$ by using the algorithm

$$A_i^1 \equiv A_i^0 - \tfrac{1}{2}(M^{-1})_{ij} \frac{\partial \chi^2}{\partial A_j} . \tag{63}$$

In the eigenvalue method,[13] M_{ij} is diagonalized, and only eigenvalues of similar size are used in Eq. (63) to improve the A parameters. The algorithm steps first along large eigenvalues, and then along smaller ones. In terms of the structure of $\chi^2(A_i)$ in the A-parameter space, eigenvectors of M_{ij} with large eigenvalues correspond to regions of χ^2 with large curvature, while eigenvectors with small eigenvalues correspond to nearly flat regions. Thus, combinations of parameters corresponding to eigenvectors with small eigenvalues are not well determined by the fit. The eigenvalue method is capable of optimizing the well-determined combinations of parameters, and is insensitive to poorly determined combinations.[13,14]

We present two fits to the data in Figs. 2 and 3. We will refer to them in the following as fits numbers 1 and 2, respectively. Both have low values of χ^2/DF. They are 0.74 and 0.95, respectively. 0.74 was the lowest value of χ^2/DF which we obtained in our fitting efforts. The values of the parameters of these two fits are given in Table I. Although the inclusive distributions of the two fits look similar, there are some major differences between them. To understand the differences let us first study the positions of the eigenvalues of the effective Hamiltonian. Figures 4 and 5 show these positions as a function of energy on M-Γ plots for the two resonances in fit number 1. Figure 6 presents the same information about fit number 2. We note that in both fits there is one eigenvalue which ends up with a very high width.

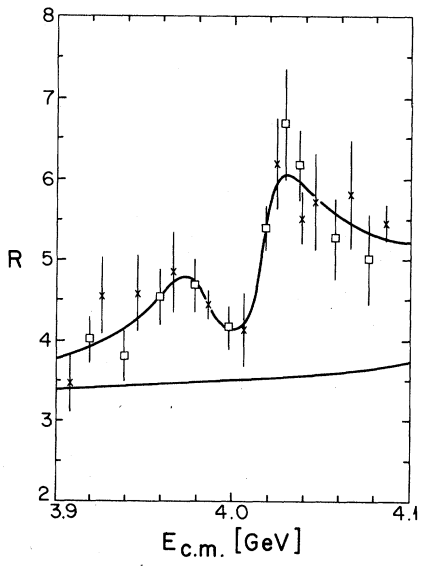

FIG. 2. Fit number 1 to inclusive SPEAR data (Ref. 5). Errors are statistical. (The background function is also shown.)

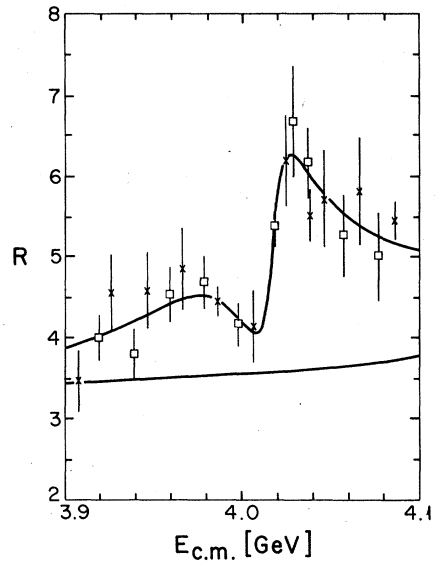

FIG. 3. Fit number 2 to inclusive SPEAR data (Ref. 5). Errors are statistical.

This is the result of imposing the constraint on the $D^*\overline{D}^*$ cross section, Eq. (54). Otherwise the two fits look quite different on the M-Γ plots. In fit number 1 the two resonances are located in different mass regions. Both resonances perform a clockwise motion in the M-Γ plane. Such a behavior is expected in a single-resonance problem under similar conditions, i.e., with a strong channel opening up inside the resonance energy domain. In Fig. 6 we see that such a clockwise motion is also true for the behavior of the average mass vs the average width of fit number 2, but the individual eigenvalues move differently. This difference is due to a strong energy dependence in the complex angle z which affects the mass and width differences [see Eq. (A5) in the Appendix] and spoils the clockwise motion.

Figure 6 looks like a level-crossing effect is taking place slightly above 4 GeV. This is confirmed by investigating the remaining parameters x and y. It is particularly useful to look at the combination defined by $\sin^2\alpha$ in Eq. (34). This is the probability of state $|1\rangle$ being found in resonance $|II\rangle$. Figure 7 shows the energy dependence of $\sin^2\alpha$ and the magnitude of the overlap between the two resonances for the two fits. We see that above 4 GeV there occurs a rapid change in the two resonances of fit number 2 and, when expressed in terms of the $|1\rangle$ $|2\rangle$ basis, they switch roles. Figure 7 complements the M-Γ plots and together they provide the complete inclusive description of the resonances. Fit number 1 does not show any

TABLE I. Parameters and results of the fits to the SPEAR data. The parameters of the fits are presented with an accuracy which is required to reproduce a good fit and does not reflect the errors in the parameters.

	Fit No. 1	Fit No. 2
M_{11}^0 (GeV)	4.4268	4.1403
M_{12}^0 (GeV)	0.1024	0.0664
M_{22}^0 (GeV)	4.0017	4.0174
α_1 (GeV$^{1/2}$)	0.5924	0.3276
α_2 (GeV$^{1/2}$)	0.1258	0.1349
b_1 (GeV$^{1/2}$)	0.3780	0.3663
b_2 (GeV$^{1/2}$)	−0.0699	−0.1253
c_1 (GeV$^{1/2}$)	0.0321	3.228×10^{-5}
c_2 (GeV$^{1/2}$)	0.1443	−0.1062
B	3.0825	3.1288
$\frac{3\pi}{f^2}$	0.0488	0.0234
$\int_{3.9}^{4.1}\Delta R\,dE$ (MeV)	258	246
ΔR_A (at E = 4.028 GeV)	1.19	1.06
ΔR_B (at E = 4.028 GeV)	1.16	1.43
ΔR_C (at E = 4.028 GeV)	0.15	0.17

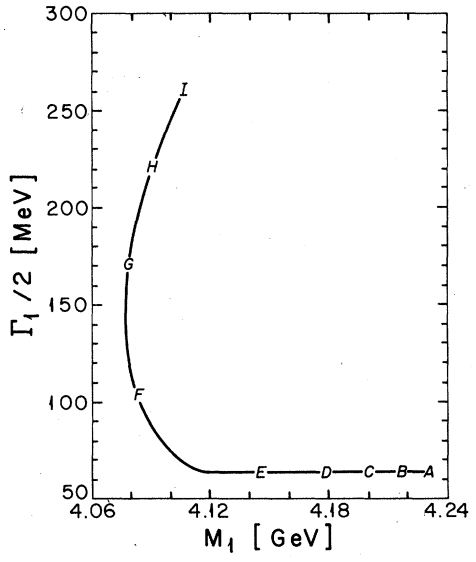

FIG. 4. The energy variation of the eigenvalues M_1 and Γ_1 of fit number 1. A, B, $\cdots$, I represent the energies 3.900, 3.925, $\cdots$, 4.100 GeV, respectively.

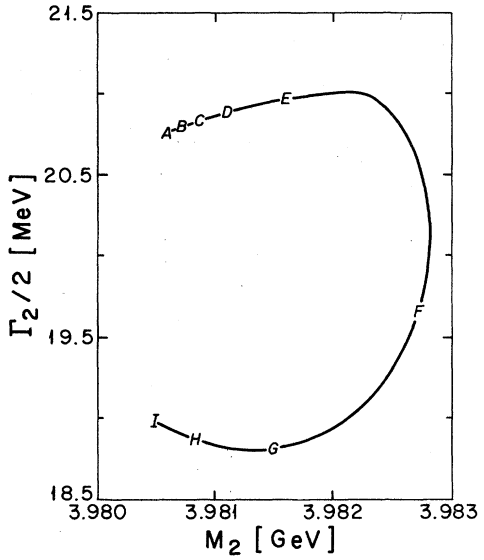

FIG. 5. The energy variations of the eigenvalues M_2 and Γ_2 of fit number 1. A, B, $\cdots$, I are as in Fig. 4.

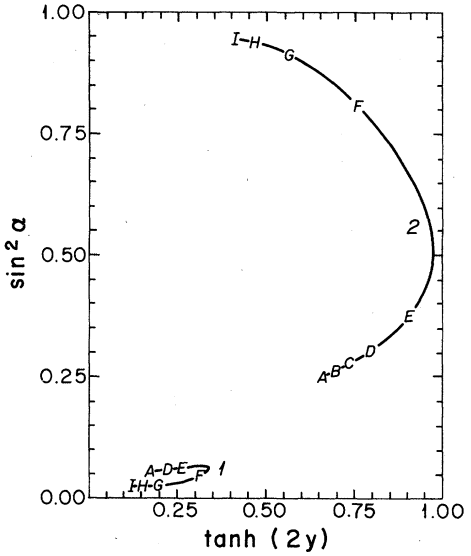

FIG. 7. Energy variation of the overlap, Eq. (12), and relative probability, Eq. (34), for both fits numbers 1 and 2. Fit number 2 shows extreme overlap as well as level crossing features after 4.0 GeV (point E). A, B, $\cdots$, I are as in Fig. 4.

surprises in Fig. 7, as expected in view of the smooth behavior of the M-Γ plots. The parameter $\sin^2\alpha$ is very important in our problem: It specifies the strength of the production of resonance $|\mathrm{II}\rangle$ since we assumed that the photon couples only to the state $|1\rangle$. Figure 7 tells us that slightly above 4 GeV the two resonances of fit number 2 are produced with the same strength

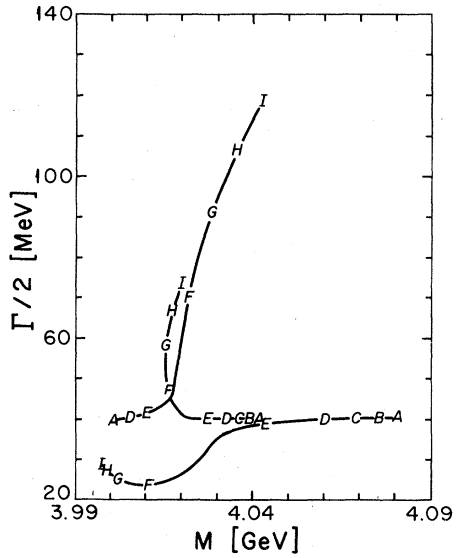

FIG. 6. M and Γ eigenvalues of fit number 2 which have level crossing features. A, B, $\cdots$, I are as in Fig. 4. The curve which shows clockwise energy behavior is the variation of the average mass and average width.

and overlap very strongly. Hence we expect to find enormous interference effects. By studying the individual decay channels we will see that this is indeed the case.

Figure 8 shows the cross section in the $D\bar{D}^* + D^*\bar{D}$ channel for fit number 1 and depicts separately the incoherent sum of the two resonances and their interference term. Figure 9 is the analogous plot for fit number 2 and it shows violent interference structure. The values of the resultant cross section (curve C in Fig. 9) are not very different from those in Fig. 8. Similar statements, though not nearly as dramatic an interference display, hold for the $D\bar{D}$ channel whose behavior is shown in Figs. 10 and 11 for the two fits. As already stated above, the strong interference behavior of fit number 2 should be expected on the basis of Fig. 7: When $|\chi|$ approaches 1 the individual terms of the cross sections blow up and only their sum is small. This is also evident from the analytic expressions of Eq. (32) and Eq. (50). The $D^*\bar{D}^*$ channel, whose main contribution comes at an energy where the overlap $|\chi|$ of fit number 2 goes down again, does not show large differences between the two fits. Figures 12 and 13 display the contribution to R of the two fits in this channel. In both cases a strong contribution occurs at 4.03 GeV, as required by the constraint of Eq. (54).

It should be emphasized that the changes in the structure of the $D\bar{D}$ and $D\bar{D}^* + D^*\bar{D}$ channels are

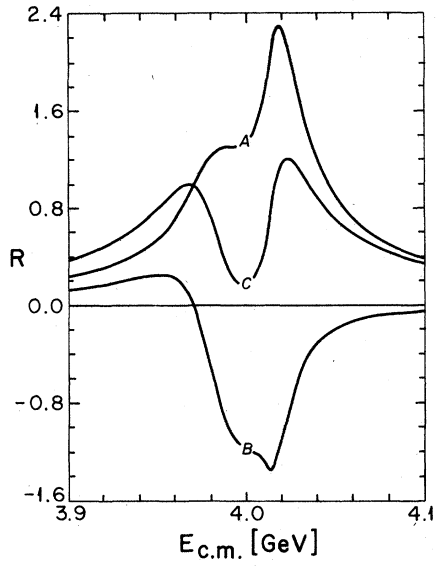

FIG. 8. The contribution to R of the channel $D\bar{D}^* + D^*\bar{D}$ for fit number 1. Curve C represents the total contribution. Curve A represents the incoherent sum of the squares of the two resonances and curve B shows their interference [see, e.g., Eq. (50)].

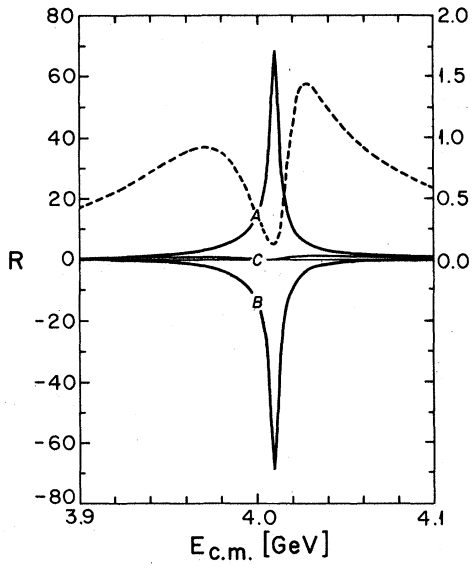

FIG. 9. The contribution to R for fit number 2 of the channel $D\bar{D}^* + D^*\bar{D}$. Notation is the same as in Fig. 8. The peaked structure in A and B is explained by tanh $2y$ approaching 1 at this energy, as evident from Fig. 7. The scale on the left refers to curve, A, B, C. The scale on the right refers to the dashed curve which is a reproduction of curve C in an expanded scale.

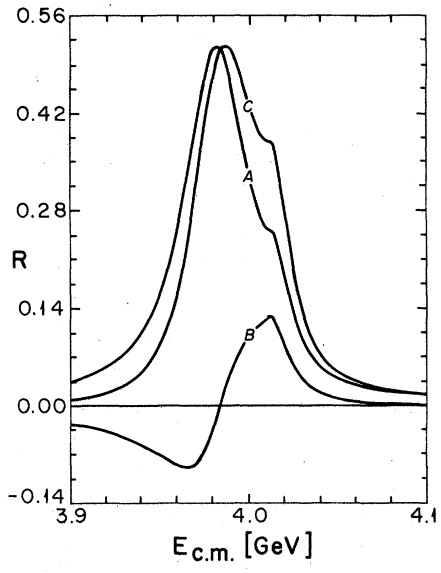

FIG. 10. The contribution to R for fit number 1 of the $D\bar{D}$ channel. Notation is as in Fig. 8.

due only to the variations in the parameters of the resonances since the coupling to these two decay channels was kept fixed. One can of course envisage a situation where the coupling amplitude itself varies with energy beyond simple analyticity requirements at threshold. This is indeed the case in the explicit charmonium model of Ref. 15. One may even find nodes in these couplings as a function of energy. In our analysis we assumed

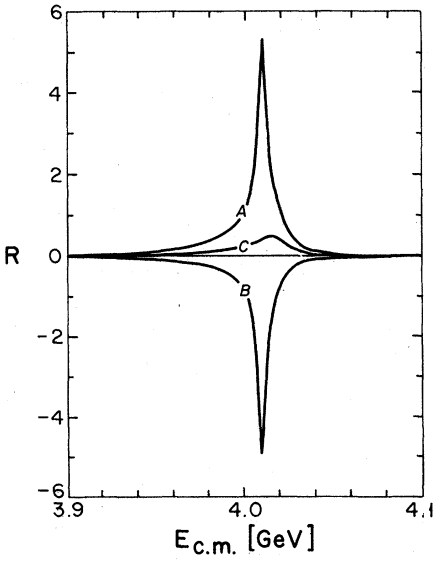

FIG. 11. The contribution to R for fit number 2 of the $D\bar{D}$ channel. Notation is as in Fig. 8.

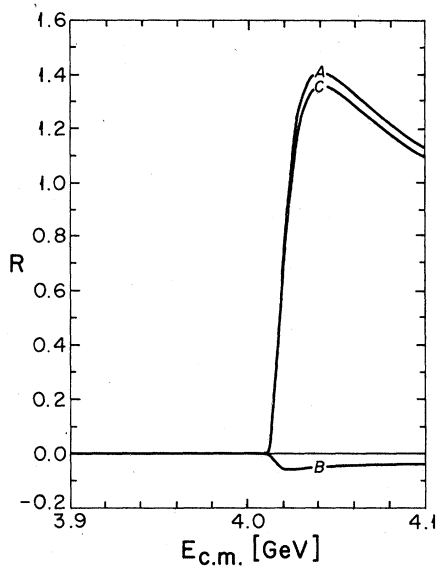

FIG. 12. The contribution to R for fit number 1 of the $D^*\bar{D}^*$ channel. Notation is as in Fig. 8.

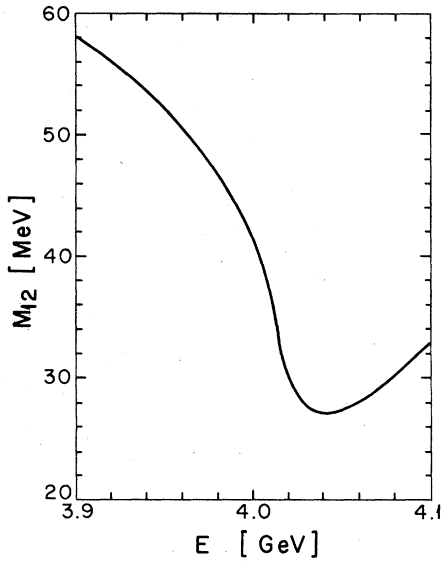

FIG. 14. M_{12} values of fit number 1.

that this is not the case, and that the energy range over which we fit is small enough to justify a constant approximation to the couplings of the resonances to these decay channels. Any other assumption would have to rely on additional information derived either from experiment or from a detailed theoretical model.

Finally we would like to present another aspect of our fits which connects the system of resonances studied in this section with the one studied in the preceding section. In Figs. 14 and 15 we present plots of M_{12} vs energy for fits numbers 1 and 2. It is interesting to note that the values of these parameters are of the same order of magnitude as the 30 MeV deduced from the ψ'-ψ'' analysis in Sec. III. This adds credibility to the assumption that both systems are of the same kind, i.e., s-d charmonium bound states.

We conclude this section with some critical observations regarding the fits that we have pre-

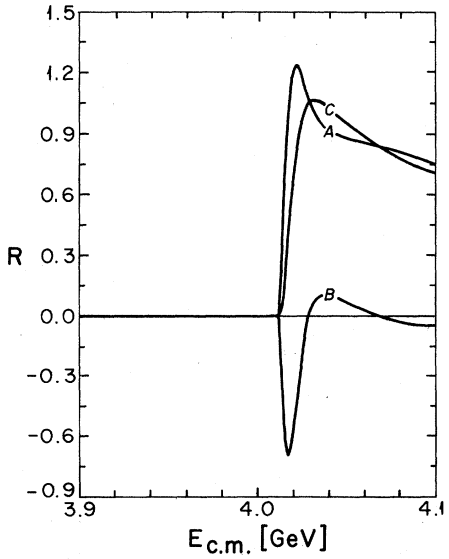

FIG. 13. The contribution to R for fit number 2 of the $D^*\bar{D}^*$ channel. Notation is as in Fig. 8.

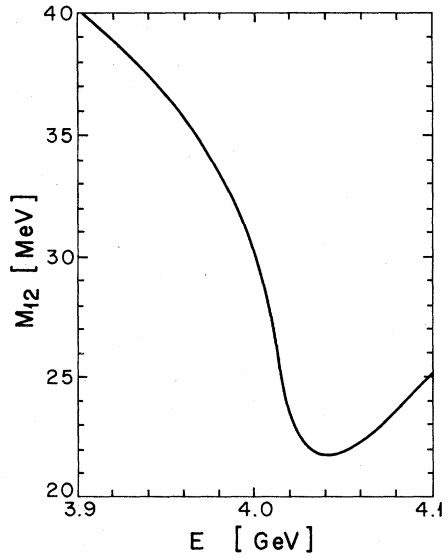

FIG. 15. M_{12} values of fit number 2.

sented. There is a lot of freedom within the range of what is considered to be a good fit, i.e., $\chi^2 \lesssim$ number of degrees of freedom. We do not consider fit number 1—or any of the many other fits that we have obtained—to be the final word in the search for a solution. More accurate data are needed to help pinpoint the correct parameters. In the meantime some ambiguity will prevail and the choice between the different kinds of fits cannot yet be made. In our fit we included the SPEAR data[8] between 3.9–4.1 GeV but have not used the two data points from the same experiment below 3.9 GeV. These are quite low and seem at odds with later SPEAR data.[5] If these points are included, they drive down the background to $B \simeq 2.4$ to 2.5. For comparison, in fit number 1, $B = 3.08$. The value of B has an important physical significance since the area of the function ΔR is related to the $\Gamma_{e^+e^-}$ of the resonance system [see Eq. (31) for narrow resonances]. An area of 100 MeV corresponds to $\Gamma_{e^+e^-}$ of 0.377 keV. If B is reduced by 0.6 then within this region alone the area is increased by 120 MeV and, therefore, the estimate of $\Gamma_{e^+e^-}$ is increased by at least 0.45 keV. The ambiguity in the value of $\Gamma_{e^+e^-}$ may, however, be much larger than that. Equation (31) holds if there is no explicit channel structure, i.e., $\underline{H}$ is a constant matrix. Otherwise one should use the value of f to determine $\Gamma_{e^+e^-} = \frac{4}{3}\pi(\alpha^2/f^2)M$ which may be different from the integral over the cross section. Moreover, our fits were driven—because of the constraint on the $D^*\bar{D}^*$ channel—to very high values of Γ at $E = 4.1$ GeV; hence the resonance structure spreads into the higher energies regime. Both effects lead to a discrepancy between the $\Gamma_{e^+e^-}$ values determined from f and the areas in the range 3.9–4.1 GeV (see Table I). Thus whereas the latter lead to a contribution to $\Gamma_{e^+e^-}$ of the order of 1 keV in both fits, we find that the proper values of $\Gamma_{e^+e^-}$ (as determined from the parameter f) are 4.6 and 2.2 keV for fits numbers 1 and 2, respectively (using $M = 4$ GeV for the resonance location). We conclude therefore that the estimate of $\Gamma_{e^+e^-}$ is subject to quite large uncertainties.

V. ANALYSIS OF DESY DATA IN THE RANGE 4.0-4.3 GeV

The available R data from DESY are not completely consistent with the R data from SPEAR. The DESY data show lower R values in the neighborhood of 4 GeV; in fact there seems to be a systematic difference of about one unit in R.[16] DESY data[17,18] are not accurate near the energy of 3.95 GeV and therefore do not corroborate the structure that we have analyzed in the preceding section. They do show a prominent resonance at 4.03 GeV and a second strong structure at about 4.16 GeV. Although SPEAR data also have an indication of another peak above 4.1 GeV, it lies at a lower mass and is much less prominent. Since it is difficult to fit both sets of data together we decided to present here different fits in separate sections. The only connection between the two is the explicit $\Delta R_{\rm HM}$ term in Eq. (55) whose parameters are determined by the analysis of the DESY data.

There exist two different sets of data from DESY—one by the DASP[17] and one by the PLUTO[18] collaborations. The DASP data are shown in Fig. 16 together with an inclusive fit in which we used ΔR as defined in Eq. (32) and assumed the background to be $B + \Delta R_\tau$ of Eq. (56). (The background contribution is explicitly shown in Fig. 16.) The fit can be specified by the values of the constant effective Hamiltonian

$$\underline{M} = \begin{pmatrix} 4.1066 & 0.0645 \\ 0.0645 & 4.1001 \end{pmatrix} \text{ GeV},$$
$$\underline{\Gamma} = \begin{pmatrix} 0.0241 & 0.0054 \\ 0.0054 & 0.0506 \end{pmatrix} \text{ GeV} \tag{64}$$

or its eigenvalues

$$M_1 = 4.1676 \text{ GeV}, \quad \Gamma_1 = 0.0421 \text{ GeV},$$
$$M_2 = 4.0391 \text{ GeV}, \quad \Gamma_2 = 0.0326 \text{ GeV}, \tag{65}$$
$$x = 0.7622, \quad y = -0.0525, \quad f = 33.38.$$

The accuracy in the various parameters, although needed to specify the fit, does not mean that the

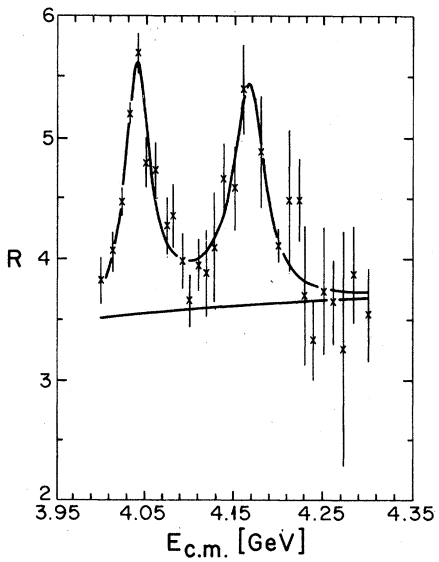

FIG. 16. Fit of Eq. (64) to DASP data (Ref. 17). Errors are statistical.

parameters are uniquely determined to the last significant figure. Other good fits can be obtained in which the matrix elements of $\underline{M}$ and $\underline{\Gamma}$ differ by a few MeV. χ^2/DF of this fit is 0.78.

The small value of y in Eq. (65) means that the overlap of the two resonances, Eq. (12), is very small. We tried therefore a fit in which y was constrained to vanish. This results in two independent BW resonances which are parametrized by

$$M_1 = 4.164\ \mathrm{GeV}, \quad \Gamma_1 = 0.046\ \mathrm{GeV},$$
$$M_2 = 4.041\ \mathrm{GeV}, \quad \Gamma_2 = 0.033\ \mathrm{GeV}, \tag{66}$$
$$f = 32.6, \quad x = 0.757.$$

In this fit $\chi^2/\mathrm{DF} = 0.80$. The matrix of Eq. (8) is now an orthogonal real matrix and $\cos^2 x$ and $\sin^2 x$ designate the amount of the state $|1\rangle$, which couples to the photon, in the two orthogonal resonance states. Since in this case there is no overlap, we can determine from the BW fits the electronic widths of the two separate resonances:

$$\Gamma^1_{e^+e^-} = 0.45\ \mathrm{keV}, \quad \Gamma^2_{e^+e^-} = 0.41\ \mathrm{keV}. \tag{67}$$

This fit looks quite similar to the one shown in Fig. 16, so we do not present a separate figure for it. The parameters of resonance number 1 in Eq. (66) and Eq. (67) were used as an input for the background of Eq. (57).

Qualitatively similar results are obtained by fitting the PLUTO data.[18] These data have quite small error bars which lead to poor values of χ^2/DF of the order of 3. We show in Fig. 17 the data together with a fit of two noninterfering resonances, i.e., constrained to have $y = 0$. This fit has the parameters

$$M_1 = 4.141\ \mathrm{GeV}, \quad \Gamma_1 = 0.082\ \mathrm{GeV},$$
$$M_2 = 4.027\ \mathrm{GeV}, \quad \Gamma_2 = 0.046\ \mathrm{GeV}, \tag{68}$$
$$x = 0.681, \quad f = 21.2.$$

The masses are slightly shifted from the values quoted in Eq. (66) owing to systematic differences between the two sets of data. The electronic widths of the two resonances are

$$\Gamma^1_{e^+e^-} = 0.81\ \mathrm{keV}, \quad \Gamma^2_{e^+e^-} = 0.53\ \mathrm{keV}. \tag{69}$$

These are higher than Eq. (67) because the background in Fig. 17 lies lower than that of the DASP fit. This happens because the fit tries to account correctly for the data points on the tail of the higher resonance which have relatively small error bars. We conclude, as in the preceding section, that the e^+e^- decay width which is given by the fit is subject to a quite large uncertainty. We note that there is a large discrepancy between the values of $\Gamma_{e^+e^-}$ obtained here and the $\Gamma_{e^+e^-}$ values obtained in the preceding section, although both should refer to the same physical system.

After completion of our work we received the final version of the DASP collaboration data.[19] Fitting these data with our inclusive formula between 4.0–4.3 GeV we find the values of the parameters

$$M_1 = 4.1623\ \mathrm{GeV}, \quad \Gamma_1 = 0.0796\ \mathrm{GeV},$$
$$M_2 = 4.0383\ \mathrm{GeV}, \quad \Gamma_2 = 0.0386\ \mathrm{GeV}, \tag{70}$$
$$x = 0.7217, \quad y = -0.0250, \quad f = 28.4.$$

This fit had a value of $\chi^2/\mathrm{DF} = 1.08$. Comparing with Eq. (65) we see that the main qualitative change is that the width of the higher resonances is broader in the new fit. This reflects itself in values for the matrix elements of $\underline{\Gamma}$ which are larger than in Eq. (64) whereas the mass matrix $\underline{M}$ stays about the same.

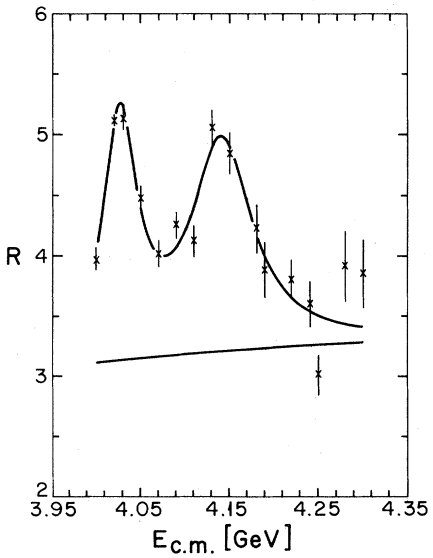

FIG. 17. Fit of Eq. (68) to PLUTO data (Ref. 18). Errors are statistical.

VI. DISCUSSION

The ideal analysis of any scattering process would involve the determination of the parameters describing a fundamental theory from which a calculation of experimental observables can be made. There would then be a formula for the value of the observables as a function of the theoretical parameters and the kinematical variables. One could then determine the best value of the parameters from a set of experimental observations. In high-energy e^+e^- annihilation, the fundamental theory is thought to be a quark bound-state model, but the dependence of the observables on a small

number of fundamental parameters is not available because of the absence of a favored quark-interaction potential. One of the goals of any analysis is therefore to help pinpoint any systematics that will control the freedom in choosing the model of quark dynamics. For example, determining systematics in the resonance spectroscopy that would limit the freedom in choosing the power dependence of the effective quark interaction potential would be a step towards eliminating many models.

In the absence of a unique set of theoretical parameters and a well-defined, calculable connection to the physical observables, a two-step process must be followed. The first step is to reduce the experimental data to a smaller set of "physically reasonable" resonance parameters. The second step is to compare these parameters to the patterns expected in various models. The first step is necessary in order to abstract from the data a finite number of pieces of information to compare to the theoretical models.

This approach is quite standard. In meson-baryon scattering, resonance parameters are abstracted, and mass patterns are subsequently identified with SU_3 or SU_6 representations. In e^+e^- annihilation, resonance parameters are also abstracted (both at low energies and above 3 GeV). In our work, we have extended these analyses to the complicated overlapping resonance structures near 4 GeV.

We presented a method for fitting inclusive and exclusive cross sections in a region of overlapping resonances and variable channel structure. This method is useful when the interference between the resonances plays a dominant role in the observed cross sections. If the resonances are well separated, or if their overlap vanishes for any other reason, the resonance system becomes an incoherent sum as discussed in Sec. V. The richness and the usefulness of the formalism becomes evident when the overlap is large, as seen in Sec. IV. Fit number 2 to the SPEAR data shows violent interference behavior in the various exclusive channels. We have seen how that is reflected in the inclusive properties of the two resonances, namely in the M-Γ and $|\chi|$ - $\sin^2\alpha$ plots. If there were no energy-dependent structure in the decay channels then those plots would reduce to points, i.e., constant choices for the parameters of the problem. Given high-accuracy data one could envisage an energy-dependent search for a smooth best fit which would lead to such plots independent of any explicit assumptions about the structure of decay channels. That would be analogous to the search for the phase-shift solution which best fits some scattering data. The analogy goes even further: M and Γ obey dispersion relations, and clockwise rotation on the M-Γ plots has the meaning of a strong local contribution to the discontinuity (Γ).

Let us turn to the physical implications of our results. In Sec. III we discussed the $\psi'(3.68)$-$\psi''(3.77)$ system and saw that it can be understood as a combination of $c\bar{c}$ s-wave and d-wave states. The s wave lies at 3.70 GeV and its photonic coupling leads to $\Gamma_{e^+e^-} \approx 2.5$ keV. This is the first excitation above the charmonium 1^{--} ground state[10] $\psi(3.1)$ which has $\Gamma_{e^+e^-} = 4.8 \pm 0.6$ keV. One higher excitation is known at 4.414 GeV with $\Gamma_{e^+e^-} = 0.44 \pm 0.14$ keV. Our analysis in Secs. IV and V covers the region between this higher excitation and the lower established ψ states.

A charmonium model[15,16] whose potential is Coulomb + linear predicts that only one $c\bar{c}$ s-wave state and two $c\bar{c}$ d-wave states lie between the ψ' and 4.4 GeV. A recent charmonium model with a logarithmic potential[20] predicts two $c\bar{c}$ s-wave states at 4.01 and 4.22 GeV with $\Gamma_{e^+e^-}$ values of 1 and 0.7 keV, respectively, in addition to several d-wave states, in the same region.

Our analyses have indicated that there are two resonances near 4 GeV, in addition to the $\psi''(3.77)$ and 4.2-GeV resonances. Thus there are at least four resonances in this energy region, more than can be accommodated by the Coulomb + linear potential model.

Our analyses of the SPEAR and DESY data in Secs. IV and V are not capable of labeling states as s-wave or d-wave quark bound states, since the quark angular momentum is a parameter in the underlying quark model and is not a parameter of the resonance description. Until $c\bar{c}$ dynamical calculations are performed which predict the complicated experimental distributions in terms of fundamental parameters, these fundamental parameters will not be determined by analyzing these experimental results. However, our analysis is able to study systematics in the resonance parameters that might be mirrored in systematics of the underlying dynamical model.

Using our analysis of the DESY data in Sec. V one can assign the two peaks to either a $c\bar{c}$ s-d system or two $c\bar{c}$ s-wave states. We have seen that an M_{12} matrix element of about 65 MeV is needed to understand these two resonance states [see Eq. (64)]. This is much larger than the analogous tensor-force term of 25–30 MeV found in the ψ'-ψ'' s-d system (as discussed in Sec. III). Within charmonium models[16] it seems difficult to accommodate a tensor force which gets larger for higher excited states. This suggests that the interpretation of the two peaks as an s-d system similar to the ψ'-ψ'' system is disfavored

relative to their identification as two $c\bar{c}$ s-wave states.

The SPEAR data which we analyzed in Sec. IV are an example of a possible $c\bar{c}$ s-d system. The large observed coupling to the $D^*\bar{D}^*$ channel does not conflict with such an interpretation and does not necessitate the introduction of the $D^*\bar{D}^*$ molecule concept.[21] If, in spite of the argument presented above, the two DESY peaks are an s-d system, then another type[22] of bound state may be needed to explain the structure of the SPEAR data. Qualitatively the results of Secs. IV and V are consistent with the interpretation of the structure around 4 GeV as a $c\bar{c}$ s-d system, and the resonance near 4.2 GeV as an additional s-wave excitation.

We can thus learn three facts about $c\bar{c}$ spectroscopy from our analysis. First, the number of resonant states is larger than that predicted by the popular Coulomb + linear potential model. Second, the systematics of the mass mixing parameter fits into a pattern of alternating s-wave and d-wave states between 3.7 and 4.2 GeV. Finally, the concept of molecular charmonium introduced[21] to understand the strong coupling to $D^*\bar{D}^*$ just above threshold is an unnecessary concept for understanding that effect, since other features (in particular the value of M_{12} in a two-resonance description of that effect) are not too different from the ψ'-ψ'' system. Hence an s-d system interpretation is still viable for understanding the observed energy dependence near 4 GeV.

Present sets of data are not yet accurate enough (or consistent with one another) to warrant drawing definitive spectroscopic conclusions. If future data continue to show rich structure we expect the new method of resonance analysis presented here to establish the spectrum of bound states and to help decipher their identities.

ACKNOWLEDGMENTS

D. H. acknowledges the hospitality of the Laboratory of Nuclear Studies at Cornell University during the period when most of this work was done. D. N. acknowledges informative discussions with D. Lüke, the hospitality of D. Leith at SLAC where part of this work was performed, and the hospitality of G. Fox at Caltech where the fitting project was completed. This research was supported in part by the Department of Energy under Grants Nos. EY-76-S-02-2220 and EY-76-C-03-0068, and in part by the National Science Foundation under Grant No. NSF-PHY77-20612.

APPENDIX

The effective Hamiltonian (1) for the two-resonance system depends on six real parameters. These parameters can be identified either with the matrix elements of the symmetric real matrices $\underline{M}$ and $\underline{\Gamma}$ in the T-invariant basis or with the complex eigenvalues ϵ_1 and ϵ_2 of the physical resonances and the complex angle $z = x + iy$ of Eq. (9). In this appendix we present the relations between these two sets of parameters.

One can write $\underline{H}$ in terms of ϵ_1, ϵ_2, and z by using Eqs. (7)–(10). The result is

$$\underline{H} = \begin{pmatrix} \epsilon_1 \cos^2 z + \epsilon_2 \sin^2 z & (\epsilon_1 - \epsilon_2) \sin z \cos z \\ (\epsilon_1 - \epsilon_2) \sin z \cos z & \epsilon_1 \sin^2 z + \epsilon_2 \cos^2 z \end{pmatrix} . \tag{A1}$$

Separating the real and imaginary parts of $\underline{H}$ we get

$$\begin{aligned}
M_{11} &= \tfrac{1}{2}(M_1 + M_2) + \tfrac{1}{2}(M_1 - M_2)\cos 2x \cosh 2y - \tfrac{1}{4}(\Gamma_1 - \Gamma_2)\sin 2x \sinh 2y , \\
M_{22} &= \tfrac{1}{2}(M_1 + M_2) - \tfrac{1}{2}(M_1 - M_2)\cos 2x \cosh 2y + \tfrac{1}{4}(\Gamma_1 - \Gamma_2)\sin 2x \sinh 2y , \\
M_{12} &= M_{21} = \tfrac{1}{2}(M_1 - M_2)\sin 2x \cosh 2y + \tfrac{1}{4}(\Gamma_1 - \Gamma_2)\cos 2x \sinh 2y , \\
\Gamma_{11} &= \tfrac{1}{2}(\Gamma_1 + \Gamma_2) + \tfrac{1}{2}(\Gamma_1 - \Gamma_2)\cos 2x \cosh 2y + (M_1 - M_2)\sin 2x \sinh 2y , \\
\Gamma_{22} &= \tfrac{1}{2}(\Gamma_1 + \Gamma_2) - \tfrac{1}{2}(\Gamma_1 - \Gamma_2)\cos 2x \cosh 2y - (M_1 - M_2)\sin 2x \sinh 2y , \\
\Gamma_{12} &= \Gamma_{21} = \tfrac{1}{2}(\Gamma_1 - \Gamma_2)\sin 2x \cosh 2y - (M_1 - M_2)\cos 2x \sinh 2y .
\end{aligned} \tag{A2}$$

The six equations of (A2) can be inverted and used to represent the eigenvalues and the angle in terms of the matrix elements. To simplify the notation let us define

$$\begin{aligned}
&A = M_{11} - M_{22} , \quad B = 2M_{12} , \quad C = \tfrac{1}{2}(\Gamma_{11} - \Gamma_{22}) , \quad D = \Gamma_{12} , \\
&K^4 = (A^2 + C^2 - B^2 - D^2)^2 + 4(AB + CD)^2 .
\end{aligned} \tag{A3}$$

It follows then that

$$
\begin{aligned}
&M_1+M_2=M_{11}+M_{22}\,,\\
&\Gamma_1+\Gamma_2=\Gamma_{11}+\Gamma_{22}\,,\\
&2\,(M_1-M_2)^2=K^2+A^2+B^2-C^2-D^2\,,\\
&\tfrac{1}{2}\,(\Gamma_1-\Gamma_2)^2=K^2-A^2-B^2+C^2+D^2\,,\\
&\sinh 4y=\frac{2(BC-AD)}{K^2}\,,
\end{aligned}
\tag{A4}
$$

$$
\sin 4x=\frac{2(AB+CD)}{K^2}\,,\quad \cos 4x=\frac{A^2+C^2-B^2-D^2}{K^2}\,.
$$

These equations do not determine the signs of M_1-M_2 and $\Gamma_1-\Gamma_2$ and the angle $2x$ is also not completely resolved. These various ambiguities are connected with one another. From Eqs. (A2) we deduce that

$$
M_1-M_2=\frac{2\sin 2x\cosh 2y M_{12}-\cos 2x\sinh 2y\Gamma_{12}}{\sin^2 2x+\sinh^2 2y}\,,
\tag{A5}
$$

$$
\Gamma_1-\Gamma_2=\frac{4\cos 2x\sinh 2y M_{12}+2\sin 2x\cosh 2y\Gamma_{12}}{\sin^2 2x+\sinh^2 2y}\,,
$$

from which it follows that the transformation

$$
2x\to 2x+\pi \tag{A6}
$$

induces the interchanges

$$
M_1\rightleftarrows M_2\,,\quad \Gamma_1\rightleftarrows\Gamma_2\,. \tag{A7}
$$

The various parameters have to obey a constraint which follows from the requirement that $\underline{\Gamma}$ be a positive-definite matrix. Using the equations (A2) one can obtain Eq. (16) of the text. The constraint reduces therefore to Eq. (15) which requires that

$$
\tanh 2y\leq\frac{(\Gamma_1\Gamma_2)^{1/2}}{[(M_1-M_2)^2+\frac{1}{4}(\Gamma_1+\Gamma_2)^2]^{1/2}}\,. \tag{A8}
$$

It should be noted that only if this constraint is obeyed will Eq. (32) be guaranteed to be positive-definite.

---

*On leave of absence from Tel Aviv University, Israel.
†Permanent address.

[1]Y. Dothan and D. Horn, Nucl. Phys. B114, 400 (1976).
[2]V. Weisskpof and E. Wigner, Z. Phys. 63, 54 (1930).
[3]Y. Dothan and D. Horn, Phys. Rev. D 1, 916 (1970).
[4]K. W. McVoy, Ann. Phys. (N.Y.) 54, 552 (1969); L. Stodolsky, Phys. Rev. D 1, 2683 (1970); R. L. Warnock, Ann. Phys. (N.Y.) 65, 386 (1971); L. Durand, Phys. Rev. D 14, 3174 (1976) and references therein.
[5]P. A. Rapidis *et al.*, Phys. Rev. Lett. 39, 526 (1977); 39, 974(E) (1977).
[6]P. M. Fishbane, D. Horn, and S. Meshkov, Phys. Rev. D (to be published).
[7]W. Bacino *et al.*, Report No. SLAC-PUB-2030, 1977 (unpublished).
[8]J. Siegrist *et al.*, Phys. Rev. Lett. 36, 526 (1976).
[9]J. E. Wiss, talk at the Fifth International Conference on Experimental Meson Spectroscopy, Boston, 1977, Report No. LBL-6723 (unpublished).
[10]G. J. Feldman and M. L. Perl, Phys. Rep. 33C, 285 (1977).
[11]R. Ayed and P. Bareyre, paper presented at the Second International Conference on Elementary Particles, Aix-en-Provence, 1973 (unpublished).
[12]M. L. Perl *et al.*, Phys. Lett. 70B, 487 (1977).
[13]G. C. Fox, computer program and Caltech report, 1968 (unpublished).
[14]D. Novoseller, Nucl. Phys. B137, 445 (1978).
[15]E. Eichten *et al.*, Phys. Rev. Lett. 36, 500 (1976).
[16]K. Gottfried, in *Proceedings pf the International Symposium on Lepton and Photon Interactions at High Energies, Hamburg, 1977*, edited by F. Gutbrod (DESY, Hamburg, 1977) and references therein.
[17]DASP collaboration, preliminary data presented at the International Symposium on Lepton and Photon Interactions, Hamburg, 1977 (unpublished).
[18]PLUTO collaboration, data presented at the International Symposium on Lepton and Photon Interactions, Hamburg, 1977 (unpublished); J. Burmester *et al.*, Phys. Lett. 66B, 395 (1977).
[19]B. Wiik (private communication); and R. Brandelik *et al.*, Phys. Lett. 76B, 361 (1978).
[20]J. L. Rosner and C. Quigg, Phys. Lett. 71B, 153 (1977).
[21]A. De Rújula, H. Georgi, and S. L. Glashow, Phys. Rev. Lett. 38, 317 (1976).
[22]M. Bander, G. L. Shaw, P. Thomas, and S. Meshkov, Phys. Rev. Lett. 36, 695 (1976); C. Rosenzweig, *ibid.* 36, 697 (1976); R. C. Giles and S.-H. H. Tye, *ibid.* 37, 1175 (1976); D. Horn and J. Mandula, Phys. Rev. D 17, 898 (1978).